IEEE Photonics Journal
An IEEE Photonics Society Publication

Open Access

High Sensitivity and High Stability Dual Fabry-Perot Interferometric Fiber-Optic Acoustic Sensor Based on Sandwich-Structure Composite Diaphragm

Volume 13, Number 2, April 2021

Wanjin Zhang
Ping Lu, *Senior Member, IEEE*
Zhiyuan Qu
Pingjie Fan
Chaotan Sima
Deming Liu
Jiangshan Zhang

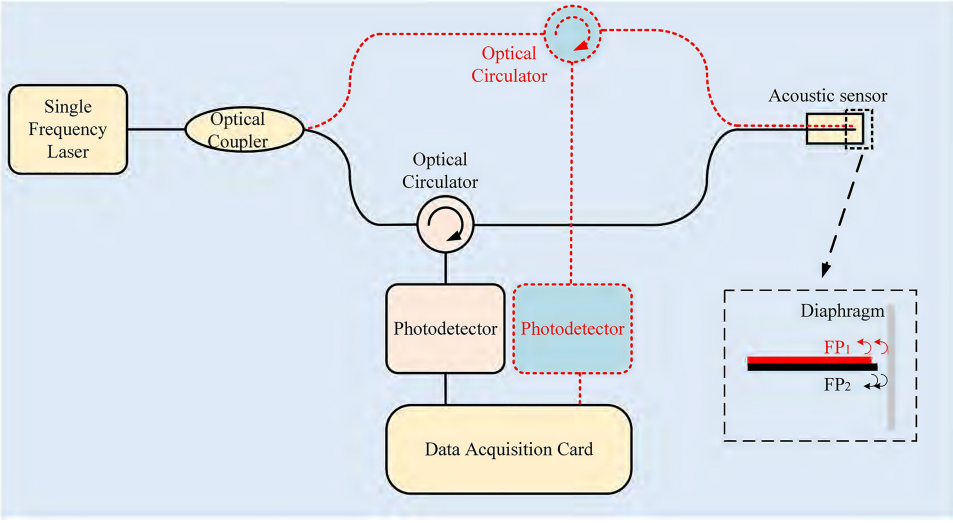

DOI: 10.1109/JPHOT.2021.3057666

High Sensitivity and High Stability Dual Fabry-Perot Interferometric Fiber-Optic Acoustic Sensor Based on Sandwich-Structure Composite Diaphragm

Wanjin Zhang,[1] **Ping Lu**,[1] ***Senior Member, IEEE***, **Zhiyuan Qu**,[1] **Pingjie Fan**,[1] **Chaotan Sima**,[1] **Deming Liu**,[1] **and Jiangshan Zhang**[2]

[1]National Engineering Laboratory for Next Generation Internet Access Systems, School of Optical and Electronic Information,Huazhong University of Science and Technology, Wuhan 430074, China
[2]Department of Electronics and Information Engineering, Huazhong University of Science and Technology, Wuhan 430074, China

DOI:10.1109/JPHOT.2021.3057666

Manuscript received November 5, 2020; revised January 8, 2021; accepted February 3, 2021. Date of publication February 9, 2021; date of current version March 4, 2021. This work was supported in part by the Natural Science Foundation of China under Grant 61775070, and in part by the Fundamental Research Funds for the Central Universities under Grants 2017KFYXJJ032, and 2019kfyXMBZ052.
Corresponding author: Ping Lu (e-mail: pluriver@mail.hust.edu.cn).

Abstract: A dual Fabry-Perot (FP) interferometric fiber-optic acoustic sensor based on sandwich-structure composite diaphragm is proposed, where fixed phase difference is generated by two FP interferometers (FPIs) with different cavity length. An ellipse fitting differential cross multiplication (EF-DCM) interrogation process is applied for phase demodulation to overcome drawbacks of quadrature point based intensity demodulation, such as temperature drifting, optical power jitter and limited dynamic range. Besides, benefiting from the large area sandwich-structure composite diaphragm, high sensitivity and wide flat frequency response are obtained. Experimental results show that phase sensitivity is -121.11 dB re 1 rad/μPa@250 Hz and sensitivity fluctuation is below 0.8 dB between 2-250Hz. To prove the high stability of the demodulation system, acoustic signal test is performed at different wavelength and different optical power and a fluctuation below 3% is observed. Moreover, profiting from the dual FP sensor structure, the acoustic sensor is get rid of influence of temperature drifting which usually leads to variation of cavity length of fiber optic acoustic sensor. The proposed sensor structure also overcomes drawbacks of traditional dual wavelength demodulation such as extra noise introduced by erbium doped fiber amplifier (EDFA) and high cost.

Index Terms: Fiber optic acoustic sensor, dual Fabry-Perot interferometers, sandwich-structure composite diaphragm.

1. Introduction

Acoustic waves exist in many situations in the world. Some of them are generated from natural processes such as volcano eruption [1], pipeline leakage [2], and partial discharge [3], [4]. Others are generated from contrived processes such as underwater communication [5], object tracking

[6], and photoacoustic imaging [7]. Frequency of the acoustic waves among them extends from infrasound to ultrasonic and hence there are pressing needs to detect such wide band acoustic signal. Diaphragm-based fiber optic acoustic sensors have attracted much interest because of their high sensitivity [8]–[10], wide frequency band [11]–[13], and high dynamic range [14]. Several diaphragms have been used to detect acoustics waves, such as metal (silver [8], [15], gold [16], [17]), two dimension materials (graphene oxide [11]), graphene [12], [13], silicon nitride [18], [19], and polymer (PPESK [20], PET [21]–[23]). Other than metal diaphragm, the rest diaphragms face the problem of low reflectivity. Metal is an ideal material for its high reflectivity, easy to be batch produced, and low cost. With the help of vacuum coating technology such as electron beam evaporation (EBE) and magnetron sputtering, high consistency and high quality diaphragm can be obtained in bulk. Gold and silver have been used to fabricate diaphragm of fiber optic acoustic sensor for their high stability. However, all of them contain single material which limits the freedom of diaphragm design in density dimension. Among diaphragm-based acoustic sensors, most of them are short cavity extrinsic Fabry-Perot interferometers which are composed of a piece of diaphragm and fiber cleaved end. For this acoustic sensors, there are several demodulation methods such as quadrature point based intensity demodulation [15], [24], [25], dual wavelength phase demodulation [21], [26], [27], 3×3 coupler phase demodulation [22], [28], three wavelength demodulation [29], [30] and spectrum demodulation [23], [31]–[34]. For quadrature point based intensity demodulation, it is low-cost and easy to realize while heavily affected by the laser wavelength, laser power and cavity length. Therefore, complicated feedback circuit is necessary to stabilize the quadrature point [20], [35], [36]. Dynamic range of quadrature point based intensity demodulation is limited by linear approximation of part of sine function, which is less than $\pi/2$ rad. For dual-wavelength phase demodulation, it is an effective method which can be used in all frequency band and is suitable for short cavity interferometer. There are several different types of methods to obtain two wavelength such as optical filters or two lasers with different wavelength. When optical filters such as polarization maintaining fiber Brag grating (PMFBG) or tunable optical filters are used, an erbium doped fiber amplifier (EDFA) is usually necessary to amplify the light from the optical filters so as to be detected by the photodetectors. In this case, unavoidable optical noise is introduced to the system. Spectrum demodulation can be used for short cavity interferometer since its spectrum is easy to be collected. With specific white-light-interference algorithm, phase change introduced by vibration of the diaphragm can be calculated precisely [37]. But for dynamic signal such as acoustic signal, high speed spectrometer is vital to collect the whole spectrum at the same time while the speed is limited to several thousand hertz. In this case, spectrum demodulation is not able to be used in high frequency acoustic signal detection. Traditional phase generated carrier (PGC) phase demodulation is not suitable for short cavity interferometer since neither internal nor external phase carrier signal can be realized [38]. For internal modulation, since modulation depth of most single frequency laser is limited to several hundreds of megahertz, it is not possible to provide enough modulation depth in short cavity interferometer. For external modulation, it is usually applied by a segment of fiber enwound around a piezoceramic while there is no fiber inside the short cavity interferometer. In conclusion, there is an acute shortage of a demodulation system which has properties of simple structure, low noise, high dynamic range and wide flat response region at the same time.

In this paper, a dual Fabry-Perot (FP) interferometric fiber-optic acoustic sensor based on sandwich-structure composite diaphragm is proposed. An ellipse fitting differential cross multiplication (EF-DCM) interrogation process is applied for phase demodulation to overcome drawbacks of quadrature point based intensity demodulation, such as temperature drifting, optical power jitter and limited dynamic range. Moreover, benefiting from the large area sandwich-structure composite diaphragm, high sensitivity and large flat frequency response are obtained. Experimental results show that phase sensitivity is -121.11 dB re 1 rad/μPa@250 Hz and sensitivity fluctuation is below 0.8 dB between 2-250Hz. To prove the high stability of the demodulation system, acoustic signal test is performed at different wavelength and different optical power and a fluctuation below 3% is observed. A temperature test is also performed to prove the stability of the fixed phase difference benefiting from the dual FP sensor structure. Compared with traditional dual wavelength

demodulation, two quadrature signals are generated from two FP interferometers (FPIs) with different cavity length instead of two different wavelengths. In this case, only one single frequency laser is used in the proposed demodulation method, which simplifies the demodulation system and decreases the cost greatly. Since power of the single frequency laser is high enough, extra EDFA is not necessary any more, which decreases the system noise greatly.

2. Sensor Fabrication and Phase Demodulation System Analysis

When the diaphragm of the fiber optical acoustic sensor vibrates along with the acoustic wave, it transforms the acoustic signal to the variation of distance between the diaphragm and fiber end face, which introduces phase change of the FPIs. In this case, vibration amplitude sensitivity of the diaphragm decides phase sensitivity of the FPIs. According to the forced vibration theory of diaphragm, vibration amplitude sensitivity and first-order resonant frequency of the diaphragm can be expressed as (1) and (2), respectively:

$$S(r) = \frac{1}{k^2 T}\left[\frac{J_0(kr)}{J_0(ka)} - 1\right], \tag{1}$$

$$f_{r1} = \frac{2.405}{2\pi a} \cdot \sqrt{\frac{P}{\rho}}, \tag{2}$$

where a, h, T, P, σ, ρ are radius, thickness, tension, tensile stress, areal density and bulk density of the diaphragm, respectively. Correspondingly, the relationships between these values can be described as $c = (T/\sigma)^{1/2}$, $T = Ph$, $\rho = \sigma/h$ and $k = \omega/c$. J_0 (kr) is zero-order Bessel function. In practice, higher sensitivity and higher resonant frequency are the goals of diaphragm design, which is realized by controlling the radius, thickness, tensile stress and density of the diaphragm. As shown in Fig. 1, when radius and tensile stress increases, sensitivity and resonant frequency present opposite change, which means a compromise has to be made between higher sensitivity and higher resonant frequency. Although thickness only influences sensitivity, thinner thickness leads to smaller dynamic ranges because linear region of vibration amplitude is limited to one third of the thickness. Lower density results in higher resonant frequency while has little effect on sensitivity. In this case, density can be used to modify resonant frequency without influencing sensitivity greatly. However, density depends on material of the diaphragm and can not be changed arbitrarily. In this case, diaphragm consisting of a single material is not capable any more. One possible way to modify the density arbitrarily is to fabricate composite diaphragm consisting of two or more materials. A three-layer composite diaphragm consisting of two materials with a sandwich structure is proposed to adjust the average density of the diaphragm so as to modify resonant frequency.

Among commonly used metal such as silver, gold, copper, aluminum (Al), titanium (Ti), chromium (Cr) and nickel (Ni), density of aluminum and titanium is much lower than the others, while aluminum is easy to be oxidized in the air and has very high coefficient of thermal expansion (CTE). On the contrary, titanium is rather stable in the air and has high strength and low CTE, while its density is slightly higher than that of aluminum. In this case, a sandwich structure with titanium-aluminum-titanium (Ti-Al-Ti) is proposed to provide lower density and higher stability. When other parameters such as radius, tensile stress, and total thickness are the same, frequency response of aluminum diaphragm, Ti-Al-Ti composite diaphragm and titanium diaphragm is shown in Fig. 2. In this simulation, thickness of aluminum and titanium is 800 nm, while in Ti-Al-Ti composite diaphragm thickness of each layer is 200 nm, 400 nm and 200 nm, respectively. Since average density of the composite diaphragm is between aluminum and titanium diaphragm, resonant frequency of the composite diaphragm is between that of aluminum and titanium diaphragm as well. In this case, flat frequency response region of the composite layer is wider than that of titanium diaphragm. Moreover, sensitivity of these kinds of diaphragm in the flat response region is almost the same. By controlling ratio of thickness of aluminum to thickness of titanium, the resonant frequency of the composite diaphragm can be tuned between 9.68 kHz and 12.5 kHz.

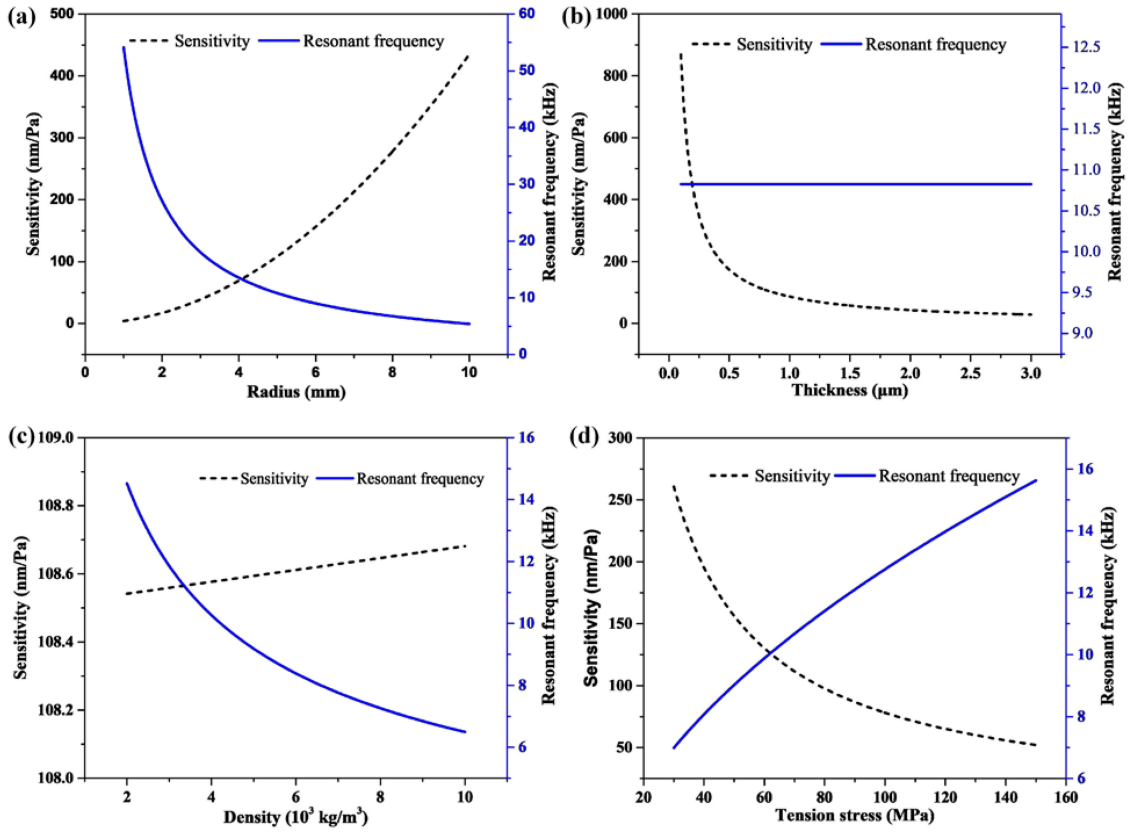

Fig. 1. Sensitivity and resonant frequency simulation.

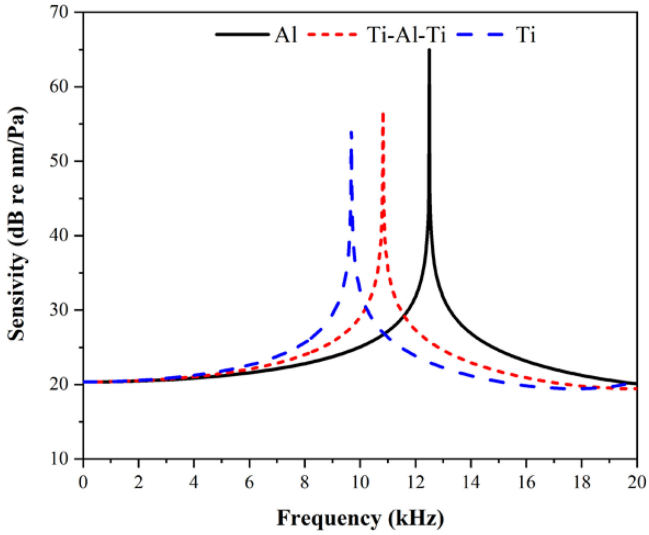

Fig. 2. Frequency response of diaphragms with different materials.

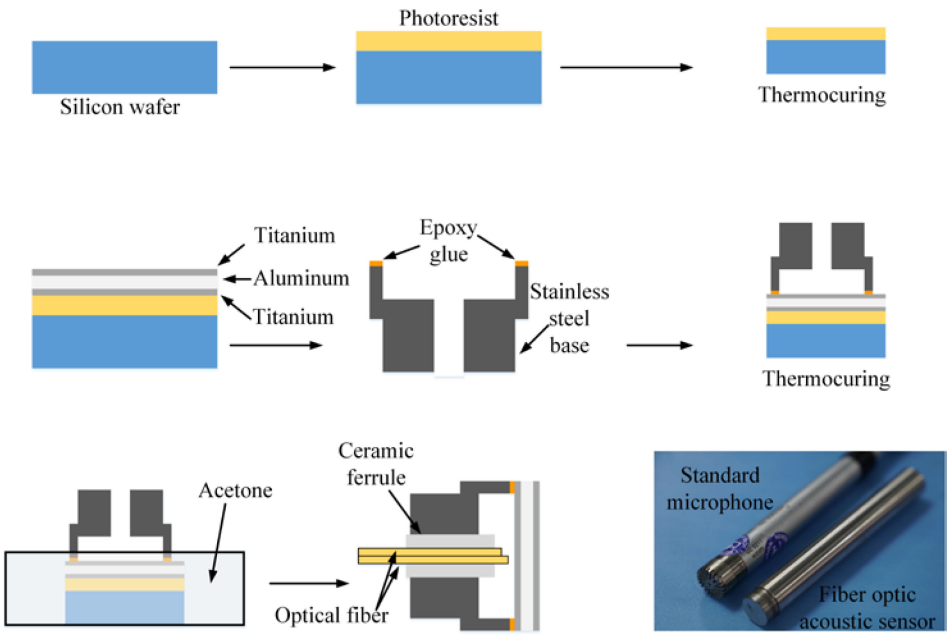

Fig. 3. Fabrication process of diaphragm.

Fabrication process of the diaphragm and sensor is shown in Fig. 3. First of all, a layer of photoresist (AZ5214) is spun on a piece of well cleaned silicon wafer and then heated on a temperature controller at 100 °C for two minutes to cure the photoresist. Then the composite diaphragm with three layers is grown on the photoresist by EBE process. To transfer the composite diaphragm from the photoresist, a stainless steel base is coated with a layer of epoxy glue (353ND) and then stuck with the composite diaphragm. To cure the epoxy glue, the diaphragm and the stainless steel base is heated on the temperature controller at 80 °C for an hour. After heating, the diaphragm and the stainless steel base is put in a culture dish containing acetone to dissolve the photoresist. Finally, two parallel and closely adjacent fibers are inserted to a ceramic ferrule. Two Fabry-Perot interferometers are formed by two fiber end faces and the metal film. Spectra of two FPIs are shown in Fig. 4 and cavity lengths of two FPIs are 161.23 μm and 600.85 μm, respectively.

Since two parallel fibers are inserted to a ceramic ferrule to form two FPIs, a simulation is made to prove that light of two FPIs will not interfere with each other. As shown in Fig. 5, the composite diaphragm is regarded as a total reflection mirror, therefore two parallel fibers are placed in a symmetric position relative to the mirror. In this case, light reflected by the composite diaphragm can be replaced by the light coupled to fibers at the symmetric position relative to the composite diaphragm.

Distances of two groups of fibers are set as 300 μm and 1200 μm, respectively, which are almost twice of lengths of two FPIs. As can be seen from Fig. 6, no matter which incident light is injected in, intensity of the emergent light coupled to the other fiber is almost zero and can be neglected. Two closely adjacent fibers ensure the same variation of two FPIs cavity lengths and short cavity length ensures that no interference will occur between two FPIs. Cavity lengths of these two FPIs are slightly different and can be controlled precisely by adjusting on a five-axis alignment jig.

Based on the dual FPI fiber optic acoustic sensor, a phase demodulation system is proposed. As shown in Fig. 7, light from single frequency laser (SFL) is separated equally by a 1×2 optical coupler. Both output ports of the optical coupler are connected to two optical circulators' first port, respectively. The second ports of those two optical circulators are connected to two Fabry-Perot interferometers of the fiber optic acoustic sensor, respectively. The third ports of two

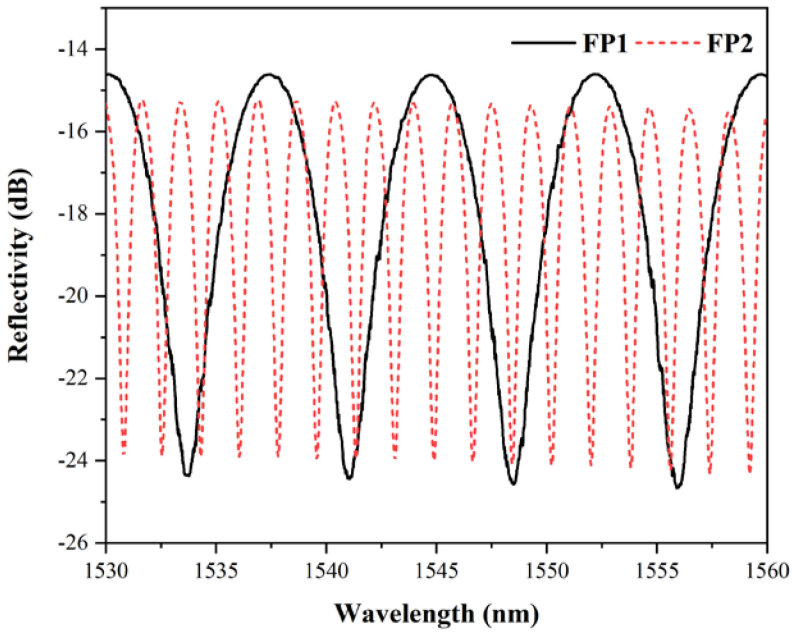

Fig. 4. Spectra of two FPIs.

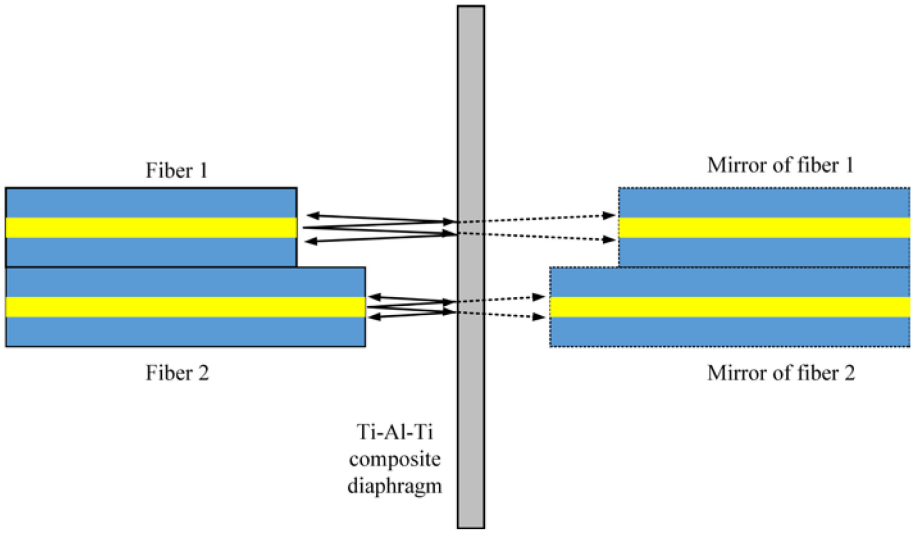

Fig. 5. Simulations of beam propagation in two FPIs.

optical circulators are connected to two photodetectors (PD), respectively. In this case, two signals from two FPIs are separately collected and will not interfere with each other.

For each photodetector, it receives one extrinsic Fabry-Perot interferometric signal. Output voltage signals of those two photodetectors can be expressed as:

$$V_1 = A_1 + B_1 \cos\left[\frac{4\pi nL_1}{\lambda} + \varphi(t)\right]$$
$$V_2 = A_2 + B_2 \cos\left[\frac{4\pi nL_2}{\lambda} + \varphi(t)\right], \quad (3)$$

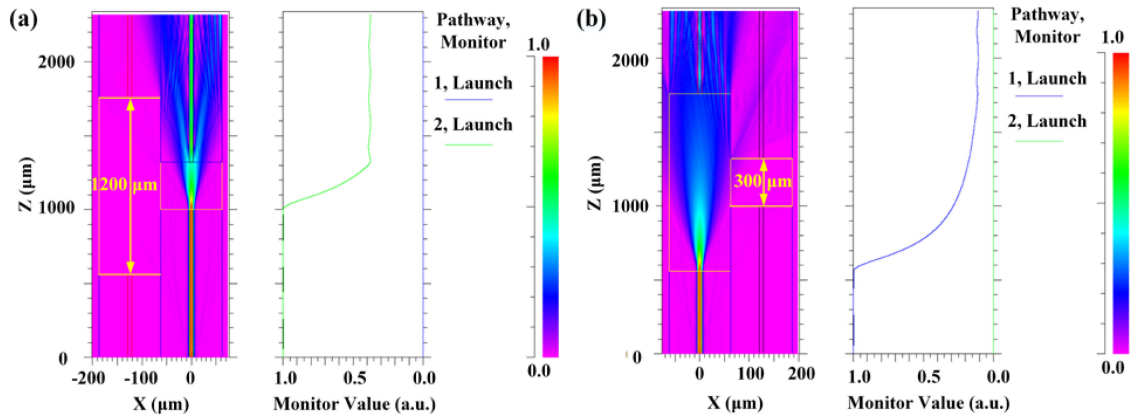

Fig. 6. Simulations of beam propagation in two FPIs.

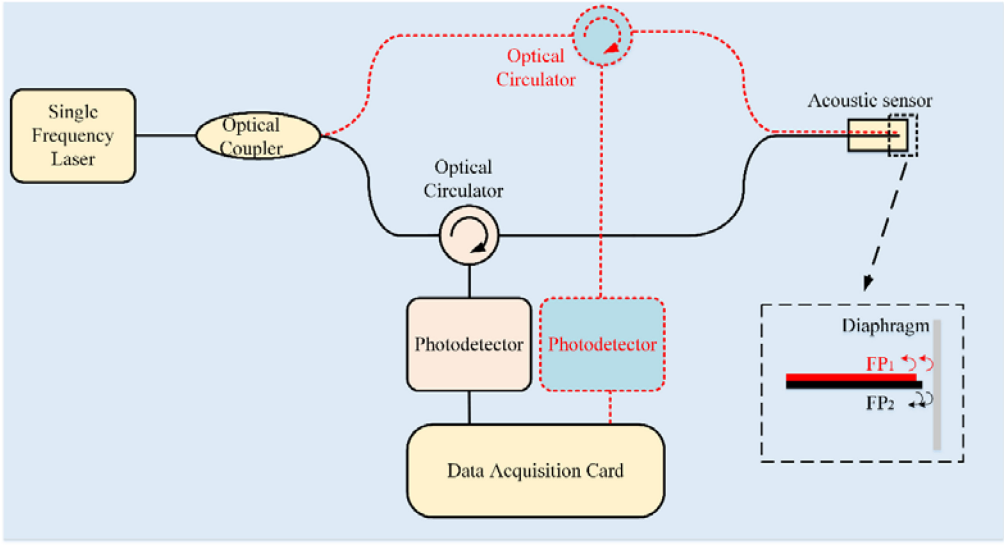

Fig. 7. System schematic.

where A_1, A_2, B_1 and B_2 are constants that are determined by those two FPIs and photodetectors. L_1 and L_2 are cavity lengths of those two FPIs. n is refractive index of the air, λ is laser wavelength and $\varphi(t)$ is phase change introduced by acoustic signal. Phase difference of those two FPIs can be expressed as:

$$\Delta\varphi = \frac{4\pi n(L_1 - L_2)}{\lambda}, \tag{4}$$

By controlling cavity length difference of those two FPIs precisely, $\Delta\varphi$ can be controlled to odd times of $\pi/2$. When cavity lengths of those two FPIs vary with temperature, their cavity length difference can stay constant, which makes the phase difference of those two FPIs stay constant accordingly.

Plotting V_1, V_2 as x, y in the coordinate system, all points will locate on an ellipse. Equation of the ellipse can be expressed as:

$$V_1{}^2 + a_1 V_2{}^2 + a_2 V_1 V_2 + a_3 V_1 + a_4 V_2 + a_5 = 0, \tag{5}$$

where a_i (i = 1, 2, 3, 4, 5) are unknown coefficients. By using ellipse fitting method, these unknown coefficients can be determined. Moreover, combining (3) (4) and (5) and eliminating $\varphi(t)$, relationship between constants in (3) and coefficients in (5) can be expressed as:

$$\begin{aligned} A_1 &= \frac{-2a_2A_2 - a_4}{a_1} \\ B_1 &= \sqrt{\left[A_1^2\left(1 - \frac{a_1^2}{4a_2}\right) + \left(A_2 + \frac{A_1a_1}{2a_2}\right)^2 - a_5\right] \Big/ \left(1 - \frac{a_1^2}{4a_2}\right)} \\ A_2 &= \frac{2a_4 - a_1a_3}{a_1^2 - 4a_2} \\ B_2 &= \frac{B_1}{\sqrt{a_2}} \\ \sin(\Delta\varphi) &= \sqrt{1 - \frac{a_1^2}{4a_2}}, \end{aligned} \tag{6}$$

After calculating constants in (3) with ellipse fitting method, output signals of two photodetectors can be normalized by eliminating direct current component and alternating current amplitude. Normalized signals can be expressed as:

$$\begin{aligned} V_{1\_norm} &= (V_1 - A_1)/B_1 = \cos\left[\frac{4\pi nL_1}{\lambda} + \varphi(t)\right] \\ V_{2\_norm} &= (V_2 - A_2)/B_2 = \cos\left[\frac{4\pi nL_2}{\lambda} + \varphi(t)\right], \end{aligned} \tag{7}$$

Differential cross multiply (DCM) method can be applied to those two normalized signals and φ(t) can be calculated as:

$$\varphi(t) = \frac{\int (V'_{1\_norm}V_{2\_norm} - V_{1\_norm}V'_{2\_norm})dt}{\sin(\Delta\varphi)}, \tag{8}$$

As long as $\Delta\varphi$ is not equal to integer times of π, ellipse fitting method and DCM method are available and $\varphi(t)$ can be calculated from (8). Moreover, there is no strict constriction that $\Delta\varphi$ has to be odd times of $\pi/2$. From the deduction above, conclusions can be drawn that dynamic range of the proposed phase demodulation system is not constrained like the quadrature point based intensity demodulation and frequency of acoustic signal to be measured is not limited as well since there is no need of carrier signal or spectrum acquisition module, which usually limits the upper frequency of the demodulation system. In this case, the proposed demodulation method can be applied to all frequency band acoustic signal detection, from infrasound to ultrasonic.

3. Experimental Results and Discussions

Fiber optical acoustic sensor testing system is shown in Fig. 8. Wavelength of SFL (NKT Photonics, X15) is tuned to 1550 nm. Light signals reflected from FPIs are collected and converted to voltage signals by two photodetectors (New Focus, 1623) respectively. Each photodetector is connected to an input port of signal analyzer (B&K LAN-XI 3160), where the voltage signal is converted to digital signal. Acoustic signal is generated by the low frequency coupler (B&K WB-3570), whose upper limit of generated acoustic signal is 251Hz and the acoustic sensor is sealed inside it. When sound pressure inside the low frequency coupler is 1.1 Pa and frequency is 250 Hz, collected voltage signals are shown in Fig. 9(a). Since phase change introduced by acoustic signal is big enough, obvious distortion is observed on both voltage signals. These distortions appear when phase change of FPIs is big enough because interferometric spectrum of FPI is a cosine function instead of a linear function. Moreover, these distortions depend on initial phase of FPIs as well

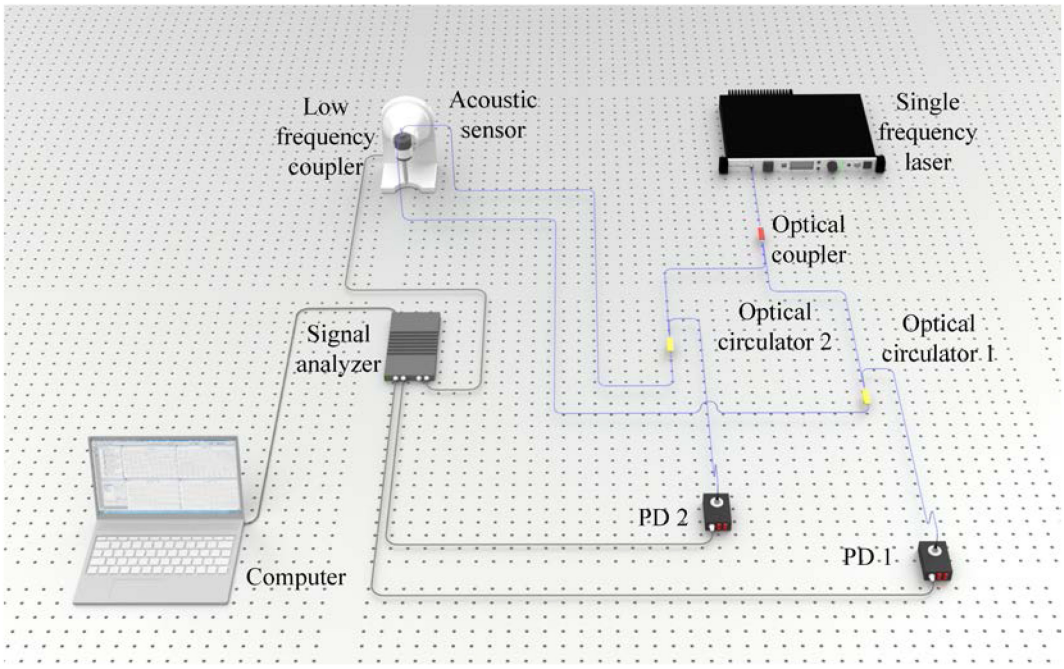

Fig. 8. Fiber optical acoustic sensor testing system.

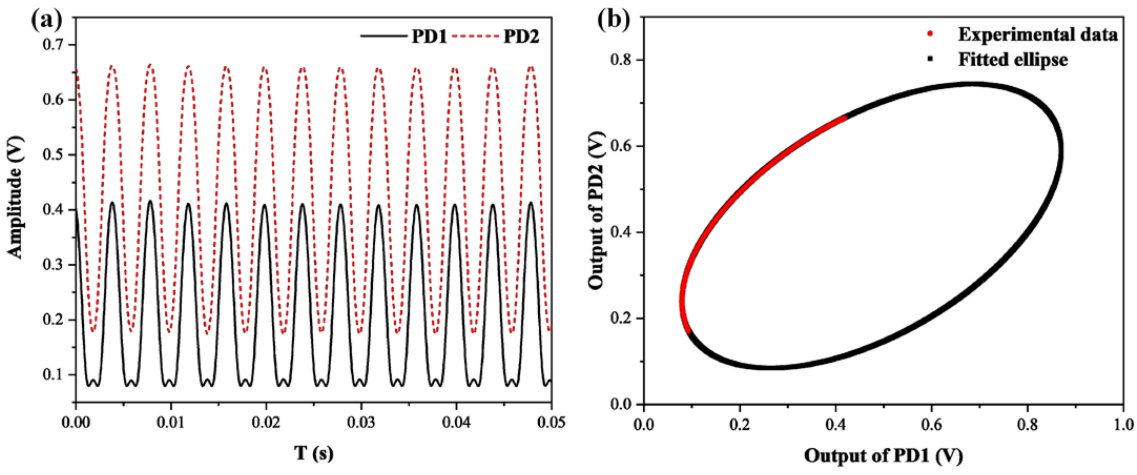

Fig. 9. (a) Signals from two photodetectors. (b) Scatter diagram and fitted ellipse.

and this can explain why significant distortion appears in signal from PD1 instead of both signals. In Fig. 9(b), distortions in signal from PD1 lead to curve of experimental data bending towards x axis. Furthermore, these distortions are supposed to appear and they make contributions to both ellipse fitting algorithm and DCM algorithm. As demonstrated in Fig. 9(b), when collected voltage signals are plotted in the coordinate system, all points will locate on an ellipse. The ellipse is not intact because sound pressure is not big enough and phase change introduced by acoustic signal is smaller than π. Moreover, major axis of the ellipse is not parallel to axis of the coordinate system, which results from that phase difference of two FPIs is not equal to odd times of $\pi/2$.

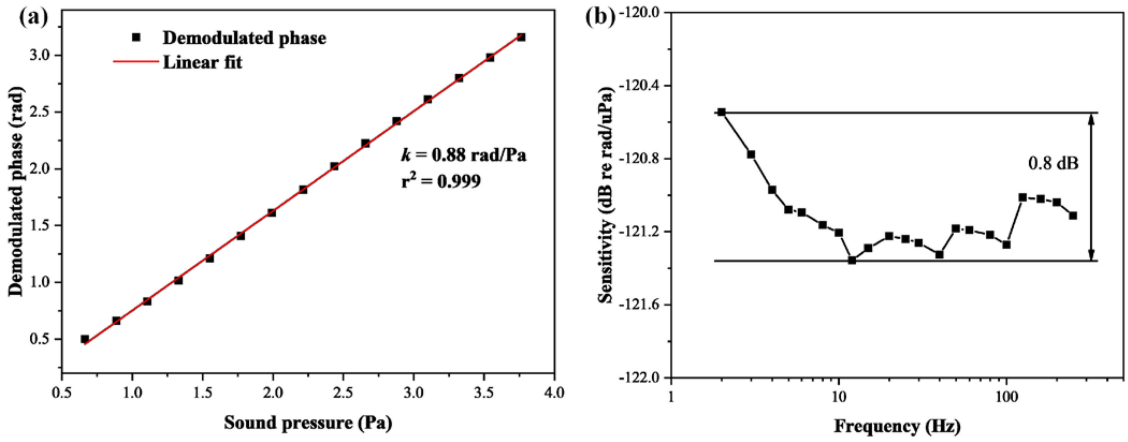

Fig. 10. (a) Linear response of optical fiber acoustic sensor. (b) Frequency response of optical fiber acoustic sensor.

Collected voltage signals are converted to digital data. Both ellipse fitting and DCM algorithm are performed based on matlab program. To evaluate linearity of the proposed phase demodulation method, phase demodulation is performed under different sound pressure. Linear response to sound pressure of the acoustic sensor is demonstrated in Fig. 10(a), in which a linearity close to 1 is obtained. Phase sensitivity of the acoustic sensor is 0.88 $\pm$ 0.005 rad/Pa. Higher sound pressure is not applied to the acoustic sensor because it exceeds linear region of the diaphragm in the acoustic sensor and might cause unrecoverable damage to the diaphragm. For intensity-based quadrature point demodulation, dynamic range is not more than $\pi/2$, while dynamic range of the proposed demodulation system can reach to as high as 3 rad. To test the frequency response characteristic of the optical fiber acoustic sensor, sensitivity test is performed between 2 to 250 Hz at one third octave. As shown in Fig. 10(b), a flat frequency response is obtained with a fluctuation of 0.8 dB. This proves that the proposed demodulation system works well at both low frequency and high frequency.

To prove that the phase difference of two FPIs is not necessary to be odd times of $\pi/2$, experiment is performed under different laser wavelength since the phase difference is related to laser wavelength and cavity length difference of two FPIs as shown in (4). During this experiment, applied sound pressure is 3.3 Pa and laser power is the same. As is illustrated in Fig. 11(a), when laser wavelength varies from 1549.8 nm to 1550.6 nm, demodulated phase varies between 2.75 rad and 2.86 rad, which can be ignored. Moreover, calculated phase difference of two FPIs varies from 0.45 rad to 1.52 rad during this experiment. As shown in that figure, calculated phase difference is highly coincident with theoretical phase difference. Slightly error mainly comes from error of calculated length difference of FPIs. In this case, as long as phase difference of two FPIs is not equal to integer times of π, the proposed dual FP phase demodulation method can work well. Furthermore, the laser power is taken into consideration since the quadrature point based intensity demodulation is highly affected by it. As is illustrated in Fig. 11(b), the lase power is adjusted from 6 mW to 15 mW, while the demodulated phase amplitude changes from 2.77 rad to 2.85 rad, where the reference error is 3%, which is much smaller than variation of the laser power. Although the demodulated phase amplitude is not related to the laser power from the former theory, high laser power provides with higher data precision, which makes the demodulated phase amplitude closer to the true value.

To prove that the proposed dual FPIs sensor structure is rid of temperature influence, temperature test is performed from 19 °C to 26 °C. As shown in Fig. 12(a), the acoustic sensor is placed on the thermoelectric controller (TEC) and spectrums of two FPIs are collected by an optical spectrum analyzer (OSA). Since cavity length of the proposed two FPIs is proportional to the phase of two

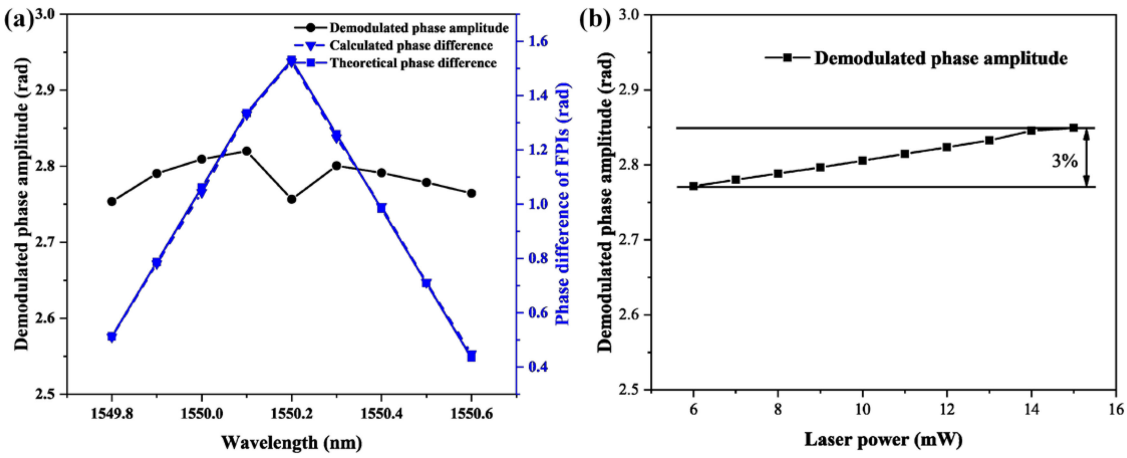

Fig. 11. Demodulated phase amplitude at (a) Different laser wavelength. (b) Different laser power.

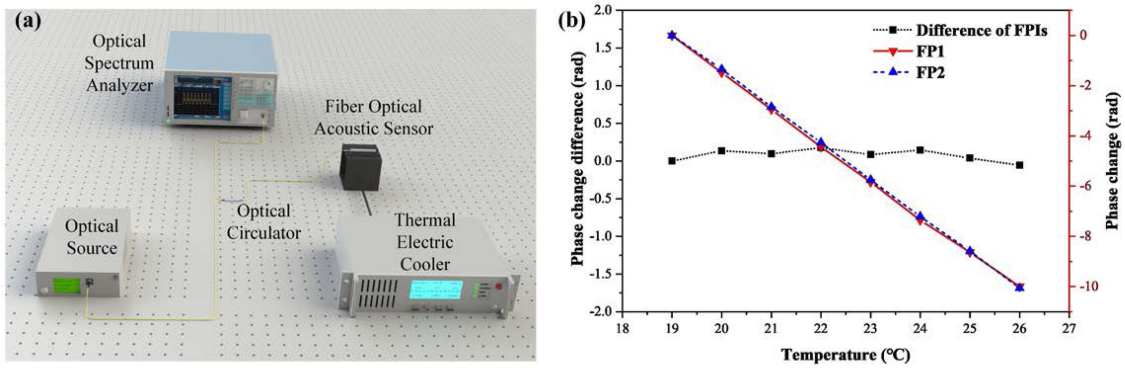

Fig. 12. (a) Temperature testing system. (b) Calculated phase change of two FPIs and phase difference of two FPIs.

FPIs, cavity length change can be calculated by the phase change. A fast Fourier transformation based white light interference demodulation [37] is used to calculate phase changes of two FPIs introduced by temperature accurately. Then phase difference of two FPIs is calculated. As shown in Fig. 12(b), when temperature changes, phase changes of two FPIs vary from 0 to 10.06 rad while phase difference of two FPIs stays relatively stable. This is consistent to the theory that phase of FPI is influenced by cavity length that is related to temperature while phase difference of FPIs is influenced by cavity length difference where temperature influence is eliminated by difference. Compared with traditional dual wavelength demodulation, dual FP phase demodulation is not affected by temperature drifting and can be applied to complex environment.

4. Conclusion

In conclusion, this paper illustrates a dual FP interferometric fiber-optic acoustic sensor based on sandwich-structure composite diaphragm. Combined with the EF-DCM interrogation algorithm, a simple, cost-saving and stable phase demodulation system is obtained. Benefit from the sandwich structure of titanium and aluminum, a stable and large area diaphragm is fabricated. In this case, phase sensitivity reaches as high as -121.11 dB re 1 rad/μPa@250 Hz and sensitivity fluctuation is below 0.8 dB between 2-250 Hz. Dynamic range of the proposed phase demodulation system

is also much higher than the traditional quadrature point based intensity demodulation. Besides, the proposed phase demodulation system overcomes the drawback of traditional dual wavelength demodulation that phase difference of two FPIs should be odd times of $\pi/2$. When laser wavelength is tuned between 1549.8 nm and 1550.6 nm to change phase difference of two FPIs, the phase demodulation system can work properly. Amplitude of the demodulated phase signal varies little compared with the fluctuation of phase difference of two FPIs. Moreover, phase demodulation is performed at different optical power. Experimental result shows that demodulated phase is hardly affected by optical power variation. Owing to the dual FP sensor structure, temperature influence to cavity length of FPIs is eliminated as well benefiting from the sensor structure of two FPIs and cost of the whole system and system noise are both reduced without using optical amplifier.

References

[1] R. S. Matoza *et al.*, "Local, regional, and remote Seismo-acoustic observations of the april 2015 VEI 4 eruption of calbuco volcano, chile," *J. Geophys. Res.-Solid Earth*, vol. 123, no. 5, pp. 3814–3827, 2018.

[2] G. S. Mothe, Y. H. Dandawate, and V. Achwal, "Signal processing system design for acoustic emission signatures detetction and analysis," in *Proc. 2nd IEEE Int. Conf. Recent Trends Electron., Inf. Commun. Technol.*, pp. 1373–1378, 2017.

[3] S. Ahmadi, M. R. Naghashan, and M. Shadmand, "Partial discharge detection during electrical aging of generator bar using acoustic technique," in *Proc. IEEE Int. Symp. Elect. Insul.*, 2012, pp. 576–578.

[4] P. Kundu, N. K. Kishore, and A. K. Sinha, "Wavelet based fractal analyzing method of partial discharge acoustic emission signal," in *Proc. Int. Conf. Ind. Inf. Syst.*, 2007, pp. 357–360.

[5] W. Xiao-yan, Z. Zhi-feng, and F. Shi-liang, "Noncooperative detection and parameter estimation of underwater acoustic DSSS-BPSK signal," in *Proc. 14th Int. Conf. Mechatronics Mach. Vis. Pract.*, 2007, pp. 52–56.

[6] D. Angela, C. Ion, I. Cornel, B. Diana, and P. Teodor, "Underwater object tracking using time frequency signatures of acoustic signals," in *Proc. Conf. OCEANS*, Taipei, 2014, pp. 1–5.

[7] M. Zhou, H. Xia, H. Zhong, J. Zhang, and F. Gao, "A noise reduction method for photoacoustic imaging in vivo based on EMD and conditional mutual information," *IEEE Photon. J.*, vol. 11, no. 1, Feb. 2019, pp. 1–10.

[8] F. Xu, J. Shi, K. Gong, H. Li, R. Hui, and B. Yu, "Fiber-optic acoustic pressure sensor based on large-area nanolayer silver diaghragm," *Opt. Lett.*, vol. 39, no. 10, pp. 2838–2840, 2014.

[9] S. Wang *et al.*, "An infrasound sensor based on extrinsic fiber-optic Fabry–Perot interferometer structure," *IEEE Photon. Technol. Lett.*, vol. 28, no. 11, pp. 1264–1267, Jan. 2016.

[10] F. Guo, T. Fink, M. Han, L. Koester, J. Turner, and J. Huang, "High-sensitivity, high-frequency extrinsic Fabry-Perot interferometric fiber-tip sensor based on a thin silver diaphragm," *Opt. Lett.*, vol. 37, no. 9, pp. 1505–1507, 2012.

[11] Y. Wu *et al.*, "A highly sensitive fiber-optic microphone based on graphene oxide membrane," *J. Lightw. Technol.*, vol. 35, no. 19, pp. 4344–4349, 2017.

[12] W. Ni *et al.*, "Ultrathin graphene diaphragm-based extrinsic Fabry-Perot interferometer for ultra-wideband fiber optic acoustic sensing," *Opt. Exp.*, vol. 26, no. 16, pp. 20758–20767, 2018.

[13] J. Ma, W. Jin, H. Xuan, C. Wang, and H. L. Ho, "Fiber-optic ferrule-top nanomechanical resonator with multilayer graphene film," *Opt. Lett.*, vol. 39, no. 16, pp. 4769–4772, 2014.

[14] L. Liu *et al.*, "UV adhesive diaphragm-based FPI sensor for very-low-frequency acoustic sensing," *IEEE Photon. J.*, vol. 8, no. 1, Feb. 2016, Art. no. 6800709.

[15] B. Liu, J. Lin, H. Liu, A. Jin, and P. Jin, "Extrinsic Fabry-Perot fiber acoustic pressure sensor based on large-area silver diaphragm," *Microelectron. Eng.*, vol. 166, pp. 50–54, 2016.

[16] W. Zhang, P. Lu, W. Ni, W. Xiong, D. Liu, and J. Zhang, "Gold-diaphragm based Fabry-Perot ultrasonic sensor for partial discharge detection and localization," *IEEE Photon. J.*, vol. 12, no. 3, Jun. 2020, Art. no. 6801612.

[17] P. Fan *et al.*, "High sensitivity fiber-optic michelson interferometric low-frequency acoustic sensor based on a gold diaphragm," *Opt. Exp.*, vol. 28, no. 17, pp. 25238–25249, 2020.

[18] X. Fu *et al.*, "Micromachined extrinsic Fabry-Perot cavity for low-frequency acoustic wave sensing," *Opt. Exp.*, vol. 27, no. 17, pp. 24300–24310, 2019.

[19] Z. Qu *et al.*, "Low-frequency acoustic Fabry–Pérot fiber sensor based on a micromachined silicon nitride membrane," *Chin. Opt. Lett.*, vol. 18, no. 10, 2020, Art. no. 101201.

[20] X. Mao, X. Zhou, and Q. Yu, "Stabilizing operation point technique based on the tunable distributed feedback laser for interferometric sensors," *Opt. Commun.*, vol. 361, pp. 17–20, 2016.

[21] Q. Liu *et al.*, "Common-path dual-wavelength quadrature phase demodulation of EFPI sensors using a broadly tunable MG-Y laser," *Opt. Exp.*, vol. 27, no. 20, pp. 27873–27881, 2019.

[22] L. Liu *et al.*, "Fiber-optic michelson interferometric acoustic sensor based on a PP/PET diaphragm," *IEEE Sensors J.*, vol. 16, no. 9, pp. 3054–3058, May 2016.

[23] S. Wang *et al.*, "All-optical demodulation fiber acoustic sensor with real-time controllable sensitivity based on optical Vernier effect," *IEEE Photon. J.*, vol. 11, no. 4, Aug. 2019, Art. no. 6801911.

[24] Y. Zhao, M. Chen, F. Xia, and R. Lv, "Small in-fiber Fabry-Perot low-frequency acoustic pressure sensor with PDMS diaphragm embedded in hollow-core fiber," *Sens. Actuator A-Phys.*, vol. 270, pp. 162–169, 2018.

[25] W. Jo, O. C. Akkaya, O. Solgaard, and M. J. F. Digonnet, "Miniature fiber acoustic sensors using a photonic-crystal membrane," *Opt. Fiber Technol.*, vol. 19, no. 6, Part B, pp. 785–792, Dec. 2013.

[26] J. Xia, S. Xiong, F. Wang, and H. Luo, "Wavelength-switched phase interrogator for extrinsic Fabry–Perot interferometric sensors," *Opt. Lett.*, vol. 41, no. 13, pp. 3082–3085, 2016.
[27] H. Liao *et al.*, "Phase demodulation of short-cavity Fabry–Perot interferometric acoustic sensors with two wavelengths," *IEEE Photon. J.*, vol. 9, no. 2, pp. 1–9, Apr. 2017.
[28] J. Jia, Y. Jiang, L. Zhang, H. Gao, and L. Jiang, "Symbiosis-Michelson interferometer-based detection scheme for the measurement of dynamic signals," *IEEE Sensors J.*, vol. 19, no. 18, pp. 7988–7992, Sept. 2019.
[29] M. Schmidt and N. Fürstenau, "Fiber-optic extrinsic Fabry–Perot interferometer sensors with three-wavelength digital phase demodulation," *Opt. Lett.*, vol. 24, no. 9, pp. 599–601, 1999.
[30] Q. Liu *et al.*, "Quadrature phase-stabilized three-wavelength interrogation of a fiber-optic Fabry–Perot acoustic sensor," *Opt. Lett.*, vol. 44, no. 22, pp. 5402–5405, 2019.
[31] M. Han, Y. Zhang, F. Shen, G. R. Pickrell, and A. Wang, "Signal-processing algorithm for white-light optical fiber extrinsic Fabry–Perot interferometric sensors," *Opt. Lett.*, vol. 29, no. 15, pp. 1736–1738, 2004.
[32] C. Ma, E. M. Lally, and A. Wang, "Toward eliminating signal demodulation jumps in optical fiber intrinsic Fabry–Perot interferometric sensors," *J. Lightw. Technol.*, vol. 29, no. 13, pp. 1913–1919, 2011.
[33] Z. Yu and A. Wang, "Fast white light interferometry demodulation algorithm for low-finesse Fabry–Pérot sensors," *IEEE Photon. Technol. Lett.*, vol. 27, no. 8, pp. 817–820, 15 Apr. 15, 2015..
[34] K. Chen *et al.*, "Fast demodulated white-light interferometry-based fiber-optic Fabry-Perot cantilever microphone," *Opt. Lett.*, vol. 43, no. 14, pp. 3417–3420, 2018.
[35] J. Chen, W. Li, H. Jiang, and Z. Li, "Stabilization of a fiber Fabry–Perot interferometric acoustic wave sensor," *Optik*, vol. 124, no. 4, pp. 339–342, 2013.
[36] Q. Wang and Z. Ma, "Feedback-stabilized interrogation technique for optical Fabry–Perot acoustic sensor using a tunable fiber laser," *Opt. Laser Technol.*, vol. 51, pp. 43–46, 2013.
[37] X. Fu, P. Lu, W. Ni, H. Liao, D. Liu, and J. Zhang, "Phase demodulation of interferometric fiber sensor based on fast Fourier analysis," *Opt. Exp.*, vol. 25, no. 18, pp. 21094–21106, 2017.
[38] B. Liu, J. Lin, H. Liu, Y. Ma, L. Yan, and P. Jin, "Diaphragm based long cavity Fabry–Perot fiber acoustic sensor using phase generated carrier," *Opt. Commun.*, vol. 382, pp. 514–518, 2017.